

Dear Dr Currie,

We thank you very much for your efforts in assisting us in improving our manuscript. On behalf of all authors, I am pleased to resubmit our revised version of manuscript **Thermocline mixing and vertical oxygen fluxes in the stratified central North Sea** as an article in *Biogeosciences* within the special issue *Low oxygen environments in marine, fresh and estuarine waters*.

We have further clarified the short “process-oriented” nature of our study. This is stated in the abstract (lines 2-5, 11-14), in the introduction on section 1.4 when presenting this study (lines 91-98), in the methods on the study site section (2.1; lines 102-104) and on section 3.3, when presenting the snapshot budget (lines 327-328). In the discussion, this is clearly formulated in the introductory paragraph (lines 353-358) when discussing the special setting of the study, and in the concluding paragraph, where we state that the implications for the whole stratification period are unknown and should be addressed in future studies (lines 531-534).

As suggested, we have tuned down the speculative section of the abstract by replacing it with a single statement (lines 14-17). Section 4.4 was streamlined and shorted to be less speculative while still providing a platform for future studies.

The language and grammatical choices in the manuscript were revised to improve the flow. Redundant articles, prepositions and adverbs were removed.

We are confident that the above addition and revision further improved the readability of the manuscript.

Again, we thank the editor and reviewers for their helpful comments, and we go forward to finalizing our manuscript.

On behalf of all authors

Lorenzo Rovelli

1 Abstract

2 In recent decades, the central North Sea has been experiencing a general trend of
3 decreasing dissolved oxygen (O₂) levels during summer. To understand potential
4 causes driving lower O₂, we investigated a three-day period of summertime
5 turbulence and O₂ dynamics in the thermocline and bottom boundary layer (BBL).
6 The study focuses on coupling biogeochemical with physical transport processes to
7 identify key drivers of the O₂ and organic carbon turnover within the BBL.
8 Combining our flux observations with an analytical process-oriented approach, we
9 resolve drivers that ultimately contribute to determining the BBL O₂ levels. We report
10 substantial turbulent O₂ fluxes from the thermocline into the otherwise isolated
11 bottom water attributed to the presence of a baroclinic near-inertial wave. This
12 transient contribution to the local bottom water O₂ and carbon budgets has been
13 largely overlooked and is shown to play a role in promoting high carbon turnover in
14 the bottom water while simultaneously maintaining high O₂ concentrations. This
15 process could become suppressed with warming climate, and stronger stratification,
16 conditions which may promote migrating algal species, that could potentially shift the
17 O₂ production zone higher up within the thermocline.

19 1 Introduction

20 1.1 Hypoxia in shelf seas and coastal regions

21 The distribution of dissolved oxygen (O₂) in marine systems results from a
22 complex interaction between biological processes (photosynthesis and respiration)
23 and physical processes (O₂ flux pathways) occurring within the water column and at
24 the seafloor. O₂ is regarded as an important indicator of ecosystem functioning for
25 aquatic organisms (Best et al., 2007) and for benthic activity (e.g., Glud, 2008).
26 Changes in O₂ distribution, concentrations and supply can therefore have severe
27 impacts on shelf ecosystems. O₂ concentrations below 62.5 μmol L⁻¹, which is
28 generally regarded as the threshold of hypoxia (Vaquer-Sunyer and Duarte, 2008), are
29 shown to significantly stress aquatic communities and increase the mortality among
30 fish communities (Diaz, 2001). These ecological and economic impacts of O₂
31 depletion lead to increasing concern regarding hypoxia occurrence and hypoxic
32 events. As reviewed by Diaz and Rosenberg (2008), hypoxia in coastal environments
33 is spreading and so are the reports of unprecedented occurrence of hypoxia in several

Lorenzo Rovelli 23/12/2015 18:50

Deleted: the...potential causes driving low ... [1]

Lorenzo Rovelli 23/12/2015 18:50

Deleted: the... complex interaction between ... [2]

72 shelf seas and coastal regions (Grantham et al., 2004; Chan et al., 2008; Crawford and
73 Pena, 2013).

74

75 1.2 Hydrodynamics and oxygen depletion in the North Sea

76 The North Sea is situated on the North–West European continental shelf,
77 between the British Islands and continental Europe (Fig. 1). Its semi-enclosed basin
78 covers an area of 575'300 km², with an average depth of 74 m and a general decrease
79 in depth from North to South (Otto et al., 1990). The central region is characterized
80 by the presence of the Dogger Bank, a shallow sandbank that acts as a hydrological
81 divide. The northern and central North Sea hydrology is mainly dominated by inflow
82 from the North Atlantic Ocean at the northern open boundary, while the southern part
83 relies on inflow from the English Channel (Thomas et al., 2005). Northern and central
84 North Sea areas are characterized by seasonal water column stratification (April to
85 September - October; Meyer et al., 2011). With only weak, wind-driven residual
86 currents (Otto et al., 1990), this stratification leads to isolation of central North Sea
87 bottom water and subsequent O₂ depletion.

88 In the central North Sea, the occurrence of low O₂ levels in bottom waters has
89 been reported (e.g., North Sea Task Force, 1993; Greenwood et al., 2010). Additional
90 monitoring studies in the central North Sea in 2007 and 2008 have shown that O₂
91 concentration in bottom waters at the Oyster Grounds and North Dogger can drop to
92 163 – 169 μmol L⁻¹ (60 – 63% saturation) and ~200 μmol L⁻¹ (71% saturation),
93 respectively (Fig. 1; Greenwood et al., 2010). Comparable field observations were
94 also reported in the summer of 2010 (Queste et al., 2013). The authors also reviewed
95 the available historical O₂ data in the North Sea (1900 – 2010), revealing a clear
96 increase in O₂ depletion after 1990.

97 While the reported O₂ levels were still above the hypoxic threshold, growing
98 concerns of hypoxia developing in the North Sea have highlighted the need for more
99 detailed studies on O₂ dynamics and its driving forces (Kemp et al., 2009). Since
100 1984, surface water temperatures in the North Sea have increased by 1 – 2°C, greater
101 than the global mean (OSPAR, 2009, 2010; Meyer et al., 2011). On seasonal time
102 scales, climate projections indicate longer durations of the stratification period and
103 stronger thermocline stability (Lowe et al., 2009; Meire et al., 2013), with some
104 projections suggesting earlier onset of stratification (e.g., Lowe et al., 2009). Due to

Lorenzo Rovelli 23/12/2015 18:50

Deleted: in

Lorenzo Rovelli 23/12/2015 18:50

Formatted: Space Before: 6 pt

Lorenzo Rovelli 23/12/2015 18:50

Deleted: .

Lorenzo Rovelli 23/12/2015 18:50

Deleted: which has

Lorenzo Rovelli 23/12/2015 18:50

Deleted: .

Lorenzo Rovelli 23/12/2015 18:50

Deleted: center

Lorenzo Rovelli 23/12/2015 18:50

Deleted: also

Lorenzo Rovelli 23/12/2015 18:50

Deleted: The

Lorenzo Rovelli 23/12/2015 18:50

Deleted: also

Lorenzo Rovelli 23/12/2015 18:50

Deleted: the occurrence of

Lorenzo Rovelli 23/12/2015 18:50

Deleted: . Taken together with

Lorenzo Rovelli 23/12/2015 18:50

Deleted: can lead

Lorenzo Rovelli 23/12/2015 18:50

Deleted: that promotes

Lorenzo Rovelli 23/12/2015 18:50

Deleted: Indeed, in

Lorenzo Rovelli 23/12/2015 18:50

Deleted: already

Lorenzo Rovelli 23/12/2015 18:50

Deleted: in the past

Lorenzo Rovelli 23/12/2015 18:50

Deleted: More recently,

Lorenzo Rovelli 23/12/2015 18:50

Deleted: for the

Lorenzo Rovelli 23/12/2015 18:50

Deleted: –

Lorenzo Rovelli 23/12/2015 18:50

Deleted: period

Lorenzo Rovelli 23/12/2015 18:50

Deleted: the

Lorenzo Rovelli 23/12/2015 18:50

Deleted: as low as

Lorenzo Rovelli 23/12/2015 18:50

Deleted: the

Lorenzo Rovelli 23/12/2015 18:50

Deleted: In fact, since

Lorenzo Rovelli 23/12/2015 18:50

Deleted: projection also

129 the semi-enclosed nature of the North Sea, earlier onset and longer stratification
130 increases the length of time that deep waters are isolated, potentially allowing lower
131 O₂ concentrations to develop (Greenwood et al., 2010).

132

133 1.3. Physical drivers of oxygen dynamics

134 The distribution of O₂ and other dissolved constituents within aquatic systems
135 are largely driven by physical transport processes. These include wind driven air –
136 water gas exchange at the sea surface (Wanninkhof, 1992), molecular diffusion at the
137 sediment – water interface (Jørgensen and Revsbech, 1985), horizontal advection
138 (e.g., Radach and Lenhart, 1995) and turbulent transport in the water column, where
139 the latter transport was reported to significantly contribute to constituent balances (see
140 Rippeth, 2005; Fischer et al., 2013; Kreling et al., 2014; Brandt et al., 2015). In shelf
141 seas, the seasonal occurrence of steep thermoclines acts as an important physical
142 barrier separating the surface layer from nutrient-rich deeper waters (Sharples et al.,
143 2001). As measurements of shear and stratification have shown, the central North Sea
144 thermocline is in a state of marginal stability (van Haren et al., 1999). Hence
145 additional sources of shear could trigger shear instability leading to local production
146 of turbulence within the thermocline. This enhanced local turbulence would
147 subsequently enhance the vertical exchange of constituents such as O₂, organic carbon
148 and nutrients. Resolving processes that drive diapycnal (i.e., vertical) fluxes across the
149 thermocline throughout the stratification period is key to understanding the
150 biogeochemical functioning of shelf seas (e.g., Sharples et al., 2001).

151

152 1.4 Present study

153 The goal of this study is to provide understanding of key turbulent processes
154 driving O₂ fluxes across the thermocline during the summertime stratification period
155 in the central North Sea using data from a 3-day process study. We investigate and
156 describe O₂ dynamics and fluxes to the bottom waters and discuss their potentially
157 influence on the seasonal O₂ balance. Using the resolved O₂ fluxes, we perform a
158 simple 1-D mass balance model to quantify O₂ sources and sinks. Finally, processes
159 that could further promote hypoxia in the central North Sea in a warming climate are
160 discussed.

161

Lorenzo Rovelli 23/12/2015 18:50

Deleted: the

Lorenzo Rovelli 23/12/2015 18:50

Deleted: water is

Lorenzo Rovelli 23/12/2015 18:50

Deleted: controls on

Lorenzo Rovelli 23/12/2015 18:50

Deleted: the

Lorenzo Rovelli 23/12/2015 18:50

Deleted: dictated

Lorenzo Rovelli 23/12/2015 18:50

Deleted: the

Lorenzo Rovelli 23/12/2015 18:50

Deleted: (Wanninkhof, 1992)

Lorenzo Rovelli 23/12/2015 18:50

Deleted: ,

Lorenzo Rovelli 23/12/2015 18:50

Deleted: that

Lorenzo Rovelli 23/12/2015 18:50

Deleted:),

Lorenzo Rovelli 23/12/2015 18:50

Deleted: Therefore, resolving the

Lorenzo Rovelli 23/12/2015 18:50

Deleted: therefore

Lorenzo Rovelli 23/12/2015 18:50

Deleted: obtain a snap-shot

Lorenzo Rovelli 23/12/2015 18:50

Deleted: the

Lorenzo Rovelli 23/12/2015 18:50

Deleted: .

Lorenzo Rovelli 23/12/2015 18:50

Deleted: key processes driving the

Lorenzo Rovelli 23/12/2015 18:50

Deleted: flux

Lorenzo Rovelli 23/12/2015 18:50

Deleted: during the period of our investigation, and how this could

Lorenzo Rovelli 23/12/2015 18:50

Deleted: flux

Lorenzo Rovelli 23/12/2015 18:50

Deleted: the

Lorenzo Rovelli 23/12/2015 18:50

Deleted: , and loss in the water column.

Lorenzo Rovelli 23/12/2015 18:50

Deleted: we propose

Lorenzo Rovelli 23/12/2015 18:50

Deleted: development

186 **2 Methods**

187 **2.1 Study site**

188 We performed O_2 and turbulence measurements in the Norwegian sector of
189 the central North Sea, N. 1/9, at the Tommeliten site (56°29'30" N, 2°59'00" E; Fig. 1)
190 from 8 – 11 August 2009 aboard the R/V *Celtic Explorer* (cruise CE0913). The site,
191 located ~100 km northeast from the northern Dogger Bank, and its surroundings are
192 characterized by shallow waters (~70 m) relatively far from coastal areas (on average
193 ~300 km). The site is known for the presence of buried salt diapirs, methane (CH₄)
194 seeps and bacterial mats (Hovland and Judd, 1988). Bathymetric surveys from
195 Schneider von Deimling et al. (2010) revealed a rather flat sandy seabed with almost
196 no features, with the exception of cm-sized ripples (McGinnis et al., 2014).

197 The currents of the central North Sea are predominantly driven by the semi-
198 diurnal lunar tide (M_2) (Otto et al., 1990). Seasonal stratification begins in April
199 around Julian day 100 and lasts until the end of September or early October, Julian
200 days 270- 290 (e.g. Meyer et al., 2011). The thermocline has been identified as an
201 important zone for the establishment of primary production and the O_2 maximum
202 layer (see Pingree et al., 1978). In fact, the North Sea deep chlorophyll maximum
203 (DCM) is estimated to account for 58% of the water column primary production and
204 37% of the annual new production for the summer stratified North Sea (Weston et al.,
205 2005). The development of the associated O_2 maximum due to this production is thus
206 important and so far not considered in the overall O_2 balance of the central North Sea.

207
208 **2.2 Instrumental setup**

209 High resolution (mm scale) turbulent shear and temperature profiles were
210 obtained with a MSS90-L microstructure turbulence profiler (Sea and Sun
211 Technology, Trappenkamp, Germany). The MSS90-L is a free-falling, loosely-
212 tethered profiler which samples at 1024 Hz with 16 channels and is designed for an
213 optimal sink rate of 0.5 – 0.6 m s⁻¹. The probe was equipped with two air-foil shear
214 probes, an accelerometer (to correct for probe pitch, roll, and vibration), a fast
215 temperature sensor (FP07, 7–12 ms response time), standard CTD sensors
216 (temperature, pressure, conductivity), and a fast (0.2 s response time) galvanic O_2
217 sensor (AMT, Analysenmesstechnik GmbH, Rostock, Germany). Absolute O_2

Lorenzo Rovelli 23/12/2015 18:50
Deleted: our
Lorenzo Rovelli 23/12/2015 18:50
Deleted: campaign
Lorenzo Rovelli 23/12/2015 18:50
Deleted: over a time period of three days during the stratification period (
Lorenzo Rovelli 23/12/2015 18:50
Deleted:)
Lorenzo Rovelli 23/12/2015 18:50
Deleted: at a
Lorenzo Rovelli 23/12/2015 18:50
Deleted: long distance

Lorenzo Rovelli 23/12/2015 18:50
Deleted: :
Lorenzo Rovelli 23/12/2015 18:50
Deleted: starts
Lorenzo Rovelli 23/12/2015 18:50
Deleted: ,

Lorenzo Rovelli 23/12/2015 18:50
Deleted:) microstructure turbulence profiler.

Lorenzo Rovelli 23/12/2015 18:50
Deleted: The absolute

230 concentrations were calibrated against shipboard CTD O₂ profiles and Winkler
231 titrations using discrete water samples (see below).

232 Water column hydrodynamics were characterized with the compact benthic
233 Paleoceanography (POZ) lander, which was deployed using a video guided launcher
234 (Pfannkuche and Linke, 2003). The POZ lander recorded 3-dimensional current
235 velocity profiles and acoustic backscatter information throughout the water column
236 using a 300 kHz acoustic Doppler current profiler (ADCP; Workhorse Sentinel,
237 Teledyne RD Instruments, Poway, United States), which sampled every 15 s with a
238 bin size of 0.5 m starting from 2.75 m from the bottom. A conductivity-temperature-
239 depth (CTD) logger (XR-420 CT logger, RBR, Kanata, Canada) recorded
240 temperature, conductivity and pressure (Digiquartz, Paroscientific, Redmond, United
241 States) every 2 s near the seafloor (~0.3 m distance). The POZ lander was also
242 equipped with a Winkler-calibrated O₂ optode sensor (Aanderaa Data Instruments
243 AS, Bergen, Norway), which recorded BBL O₂ concentration at 1 min intervals.

244 Water column profiles were obtained using a SBE9plus CTD-rosette system
245 (Seabird, Washington, United States). The CTD sampled at 24 Hz and was equipped
246 with standard temperature, conductivity, pressure, O₂ and light transmission sensors.
247 The rosette system mounted 12 Niskin bottles (10 L each) for discrete water
248 sampling. Each water sample was subsampled with three Winkler bottles of known
249 volume (~62 mL on average) upon recovery, and the samples were immediately fixed
250 on deck and titrated manually within 24 h after the sampling, (see Winkler 1888).
251 CTD O₂ concentrations deviated from Winkler values by <5%.

253 2.3 Hydrodynamic data evaluation

254 The main tidal directions, (major and minor axis of the tidal ellipsoid) were
255 determined by performing a variance analysis on the ADCP velocity time series. The
256 u and v velocities were rotated over a stepwise increasing rotation angle (r) as
257 $u_{rot} = u \cdot \cos(-r) - v \cdot \sin(-r)$ and $v_{rot} = u \cdot \sin(-r) - v \cdot \cos(-r)$, and the
258 variance computed at each step. The angle with the largest variance is the main tidal
259 direction. Barotropic and baroclinic flow contributions of tides were separated by
260 least-square fitting the detrended velocity time series to harmonics $u = A \cdot \cos(\omega \cdot$
261 $t + \varphi)$ with A, ω , φ being the amplitude, frequency, and the phase lag, respectively.
262 In the analysis below, the barotropic semi-diurnal principle lunar tide (M₂) and

Lorenzo Rovelli 23/12/2015 18:50

Deleted: on

Lorenzo Rovelli 23/12/2015 18:50

Deleted: continuously

Lorenzo Rovelli 23/12/2015 18:50

Deleted: 10L-

Lorenzo Rovelli 23/12/2015 18:50

Deleted: -

Lorenzo Rovelli 23/12/2015 18:50

Deleted: depth (i.e., each Niskin-bottle)

Lorenzo Rovelli 23/12/2015 18:50

Deleted: right after

Lorenzo Rovelli 23/12/2015 18:50

Deleted: . The samples were then stored in the vessel's cold room

Lorenzo Rovelli 23/12/2015 18:50

Deleted: .

Lorenzo Rovelli 23/12/2015 18:50

Deleted: , the

Lorenzo Rovelli 23/12/2015 18:50

Deleted: ,

Lorenzo Rovelli 23/12/2015 18:50

Deleted: respectively

Lorenzo Rovelli 23/12/2015 18:50

Deleted: at

Lorenzo Rovelli 23/12/2015 18:50

Deleted: represented

277 diurnal declination tide (K_1) contributions had frequencies of 1.93227 cycles per day
 278 (cpd) and 1.00274 cpd, respectively, and were subtracted from the time series to
 279 analyze residual flow. For barotropic contributions, the fit was applied to the depth
 280 average of the time series, while baroclinic contributions were obtained by fitting the
 281 harmonics to the velocity time series from each 0.5 m ADCP bin. The occurrence of
 282 enhanced shear in the stratified water column was investigated by calculating the
 283 vertical shear of horizontal velocity, S , from the vertical gradients between adjacent
 284 bins of east and north velocity (0.5 m resolution) as $S = \sqrt{(du/dz)^2 + (dv/dz)^2}$.
 285 Frequency spectra of the time series of horizontal velocity and vertical shear of
 286 horizontal velocity were used to identify the tidal and non-tidal flow components. The
 287 spectra were calculated using fast-Fourier transforms combined with a $1/2$ -cosine
 288 taper (Hanning window), which was applied to the first and last 10% of the time
 289 series data.

290 Turbulent kinetic energy dissipation rate (ϵ) was quantified from airfoil shear
 291 readings by integrating shear wavenumber spectra assuming isotropic turbulence
 292 (Batchelor, 1953):

$$\epsilon = 7.5\mu \int_{k_{min}}^{k_{max}} E_{du'/dz}(k) dk \quad (1)$$

293 where μ is the dynamic viscosity of seawater. Shear spectra $E_{du'/dz}(k)$ were
 294 calculated from one-second ensembles (1024 values) and integrated between a lower
 295 $k_{min} = 3$ cycles per minute (cpm) and an upper wavenumber k_{min} that varied between
 296 14 cpm and 30 cpm depending on the Kolmogorov wavenumber. Here, a Bartlett
 297 window was applied to the whole ensemble prior to spectral decomposition. Loss of
 298 variance due to limited wavenumber band was taken into account by fitting the
 299 observed shear spectra to the universal Nasmyth spectrum. Similarly, corrections for
 300 the loss of variance due to finite sensor tip of the airfoil probes were applied (see
 301 Schafstall et al., 2010). The detection limit, or noise level, of the used profiler for ϵ
 302 was inferred to be 1×10^{-9} W kg⁻¹ (Schafstall et al., 2010); the upper detection limit is
 303 a function of the shear sensor geometry (up to 10^{-4} W kg⁻¹; Prandke and Stips, 1998).

304 Estimates of turbulent eddy diffusivities of mass (K_ρ) were obtained from
 305 measurements of ϵ as

$$K_\rho = \gamma\epsilon/N^2 \quad (2)$$

Lorenzo Rovelli 23/12/2015 18:50

Deleted:) that

Lorenzo Rovelli 23/12/2015 18:50

Deleted: the

Lorenzo Rovelli 23/12/2015 18:50

Deleted: the

Lorenzo Rovelli 23/12/2015 18:50

Deleted: the

310 where γ is the mixing efficiency and N^2 the water column stability. This method,
 311 proposed by Osborn (1980), approximates K_ρ under the assumption of a local
 312 equilibrium of production and dissipation of turbulent kinetic energy. Values for N^2
 313 were calculated from temperature, salinity and pressure data using the adiabatic
 314 method (Fofonoff, 1985) as $N^2 = -g(\rho^{-1}\partial\rho/\partial z - g/c^2)$, where ρ , g , and c are the
 315 density, the earth's gravitational acceleration and speed of sound. Mixing efficiency
 316 values in stratified waters range from 0.1 to 0.2 (Ivey and Imberger, 1991) and
 317 decreases in weakly stratified waters such as within the BBL (Lorke et al., 2008). To
 318 account for this decrease, we used the γ and K_ρ parameterization of Shih et al. (2005).
 319 Based on the turbulence activity parameter ε/vN^2 , with the kinematic viscosity, ν ,
 320 the authors found that in energetic regimes, i.e., $\varepsilon/vN^2 > 100$, eddy diffusivities are
 321 better estimated as $K_\rho = 2\nu(\varepsilon/vN^2)^{1/2}$. As horizontal density gradients at the study
 322 site were deemed to be small compared to vertical gradients (see Discussion), we
 323 equated diapycnal eddy diffusivities with vertical diffusivities (i.e., $K_\rho = K_z$).

324 To obtain representative mean turbulent eddy diffusivities, the data were
 325 evaluated in ensembles of three to four consecutive profiles and averaged in depth and
 326 time to reduce uncertainties due to the patchiness of turbulence, temporal fluctuation
 327 of N^2 , and temporal γ variations (see Smyth et al., 2001). As proposed by Ferrari and
 328 Polzin (2005), the level of uncertainty of the averaged K_z can be quantified as:

$$\Delta K_z = K_z \left[\left(\frac{\Delta\gamma}{\gamma} \right)^2 + \left(\frac{\Delta\varepsilon}{\varepsilon} \right)^2 + \left(\frac{\Delta N^2}{N^2} \right)^2 \right]^{1/2} \quad (3)$$

329 with Δ being the absolute uncertainty of the various average terms. Here, the
 330 uncertainties are evaluated in the region of strong vertical O_2 gradients and in 2 m
 331 depth bins. The absolute uncertainty for $\Delta\gamma$ was assumed to be 0.04 (see St. Laurent
 332 and Schmitt, 1999). The absolute uncertainty on N^2 (ΔN^2) was determined by the
 333 standard error over the 2 m average, computed as the standard deviation divided by
 334 the square root of the number of estimates. Finally, the statistical uncertainty of ε for
 335 each bin was calculated using a bootstrap method (10^4 resamples) (Efron, 1979).

336 The vertical O_2 fluxes F_θ were then obtained from K_z and the O_2 concentration
 337 gradients $\partial[O_2]/\partial z$ as

$$F_\theta = K_z \frac{\partial[O_2]}{\partial z} \quad (4)$$

338 Accordingly, the uncertainty of averaged turbulent O_2 fluxes were given by:

Lorenzo Rovelli 23/12/2015 18:50

Deleted: , respectively.

Lorenzo Rovelli 23/12/2015 18:50

Deleted: the

Lorenzo Rovelli 23/12/2015 18:50

Deleted: as well as

$$\Delta F_{\theta} = F_{\theta} \left[\left(\frac{\Delta K_z}{K_z} \right)^2 + \left(\frac{\Delta \partial_z [O_2]}{\partial_z [O_2]} \right)^2 \right]^{1/2} \quad (5)$$

342 where $\Delta \partial_z [O_2]$ denotes the standard error of mean vertical gradients of O_2
 343 concentrations. It should be noted that the analysis did not include biases or
 344 uncertainties due to measurement errors.

345

346 3 Results

347 During the three-day observational period (8 – 11 August 2009), we collected
 348 39 high-resolution MSS profiles in **consecutive** sets of three to five profiles at 5 – 10
 349 min intervals. Most of the profiles were in the evening (profiles 1 – 8, 26 – 28, 36 –
 350 39) or at night (9 – 15, 29 – 35) with the remaining profiles acquired in the morning
 351 (6 to 9 AM). One shipboard CTD profile was performed prior to the actual MSS
 352 profiles to provide hydrographic information, the water turbidity and O_2
 353 concentrations, **and** discrete water samples for subsequent onboard Winkler titrations.
 354 Hydroacoustic water column current measurements were carried out continuously
 355 throughout the observational period. The following results are structured to first
 356 present a characterization of the site's physical settings and turbulence drivers,
 357 followed by the O_2 fluxes and O_2 BBL budget.

358

359 3.1 Water column structure

360 The ~70 m deep water column was characterized by a stable, well-defined
 361 four-layer temperature structure (Fig. 2a). **The** well-mixed surface boundary layer
 362 (SBL) and bottom boundary layer (BBL), 15 m and 30 m thick, respectively, were
 363 separated by a weakly-stratified transition layer (15 – 25 m depth) and a strongly
 364 stratified interior layer (25 – 40 m depth). The stratified interior layer was
 365 characterized by two very steep thermoclines situated in the upper (27 – 30 m depth)
 366 and lower (36 – 39 m depth) region of the layer, with vertical temperature gradients of
 367 up to 4°C m^{-1} . The average salinity was 35.08 with little variation throughout the
 368 water column (35.04 – 35.1). The light transmission profile from the ship CTD ranged
 369 from 89% to 96% (Fig. 2b). The most turbid layer (89%) was observed at the lower
 370 boundary of the interior layer (at 40 m depth) suggesting the presence of the deep
 371 chlorophyll maximum, phytoplankton, zooplankton and suspended particles.

Lorenzo Rovelli 23/12/2015 18:50

Deleted:)

Lorenzo Rovelli 23/12/2015 18:50

Deleted: that were collected consecutively

Lorenzo Rovelli 23/12/2015 18:50

Deleted: collected either

Lorenzo Rovelli 23/12/2015 18:50

Deleted: as well as

Lorenzo Rovelli 23/12/2015 18:50

Deleted: A

377 The O₂ profiles were generally characterized by near saturation in the SBL
378 and transition layers (238 – 243 μmol kg⁻¹) and undersaturated (~80%) in the BBL
379 (~243 μmol kg⁻¹) (Fig. 2c,d). The stratified interior was oversaturated by up to 115%,
380 with a well-established O₂ maximum at ~39 m depth with concentrations up to ~315
381 μmol kg⁻¹. Below that maximum, at the thermocline-BBL interface, we observed a 2 –
382 3 m thick steep oxycline, with an O₂ gradient of 34 μmol kg⁻¹ m⁻¹ and exhibiting very
383 limited day/night, depth and thickness variation. We resolve the O₂ flux into the BBL
384 associated with this oxycline.

386 3.2 Hydrodynamics

387 The hydrostatic pressure dataset (POZ lander) revealed that the tidal water
388 level ranged from 0.6 to 0.9 m (Fig. 3a). Variance analysis on the ADCP velocity data
389 identified the major and minor axis of the tidal ellipsoid components to occur at 45°
390 and 135° from true north, respectively. Along these axes, the current amplitudes were
391 0.21 m s⁻¹ and 0.04 m s⁻¹, indicating a narrow tidal current ellipsoid, as reported by
392 Otto et al. (1990). The site was characterized by a negative tide polarity (anti-
393 cyclonic) for the semi-diurnal tides. A dominance of the barotropic M₂ current
394 amplitude at all depths was clearly visible in the velocity time series (Fig. 3b, c) and
395 the harmonic analyses. East (zonal) and north (meridional) barotropic M₂-current
396 amplitudes were 0.12 m s⁻¹ and 0.17 m s⁻¹, respectively, while K₁-current amplitudes
397 were only 0.005 m s⁻¹ and 0.03 m s⁻¹.

398 Although the limited length of the ADCP velocity time series did not allow for
399 full separation of the M₂ and *f* frequencies, the spectral density functions indicated
400 maximum energy at frequencies of about the semi-diurnal tide. This maximum varied
401 little with depth, indicating barotropic M₂ motions. Superimposed on those barotropic
402 currents, we observed the presence of baroclinic velocity contributions (Fig. 3b, c).
403 Additionally, near-inertial motions were also detected.

404 The occurrence of near-inertial motions was most pronounced in the
405 thermocline (32 – 39 m; Fig. 3e). Lower, but still elevated, energy densities at the
406 near-inertial band were found in the SBL and BBL. Moreover, the near-inertial
407 currents exhibited a distinct 180° phase shift between the SBL and the thermocline as
408 well as between the thermocline and the BBL, suggesting a second vertical mode
409 nature of these fluctuations. Average amplitudes of the near-inertial fluctuations in the

Lorenzo Rovelli 23/12/2015 18:50

Deleted: , with O₂ concentrations in the

Lorenzo Rovelli 23/12/2015 18:50

Deleted: range,

Lorenzo Rovelli 23/12/2015 18:50

Deleted: , where the O₂ concentration was ~

Lorenzo Rovelli 23/12/2015 18:50

Deleted: with exhibited

Lorenzo Rovelli 23/12/2015 18:50

Deleted: -

Lorenzo Rovelli 23/12/2015 18:50

Deleted: variability. With this in mind, we wish to

Lorenzo Rovelli 23/12/2015 18:50

Deleted: the

Lorenzo Rovelli 23/12/2015 18:50

Deleted: POZ lander

Lorenzo Rovelli 23/12/2015 18:50

Deleted: also

Lorenzo Rovelli 23/12/2015 18:50

Deleted: observed

Lorenzo Rovelli 23/12/2015 18:50

Deleted: observed

Lorenzo Rovelli 23/12/2015 18:50

Deleted: also

422 thermocline obtained from least-square fitting were 0.11 m s^{-1} . In the BBL and SBL,
423 average amplitudes were reduced to 0.06 m s^{-1} and 0.04 m s^{-1} , respectively,
424 suggesting that f oscillations might account for enhanced shear in the thermocline.

425 Enhanced vertical shear of horizontal velocity was found at the interior –
426 transition layer and at the interior – BBL interfacial regions (Fig. 3d). As indicated by
427 the spectral density function of the shear time series from the interior interfacial layers
428 (SI Fig. 1), the shear exhibited near-inertial frequencies (1.6722 cpd), and resulted
429 from the baroclinic near-inertial wave. The high vertical resolution (0.5 m) of our
430 velocity data allowed the resolution of the interfacial shear layers, which were
431 typically 2 to 3 m thick with elevated values of up to 0.05 s^{-1} . Comparisons with CTD
432 data showed that they are collocated with the two enhanced temperature gradients
433 layers in the thermocline ($27 - 30 \text{ m}$ and $36 - 39 \text{ m}$ depth; Fig. 2a).

434 The dissipation rates (ϵ) of turbulent kinetic energy (TKE) determined from
435 microstructure shear probes were particularly low in the center of the stratified
436 interior ($2 - 5 \times 10^{-9} \text{ W kg}^{-1}$) but still above the MSS detection limit. However, ϵ
437 increased to $5 \times 10^{-9} \text{ W kg}^{-1}$ and $2 \times 10^{-8} \text{ W kg}^{-1}$ at the upper and lower interior layer
438 limits, respectively (Fig. 4a). These coincided with the depth range of the interfacial
439 shear layers (Fig. 3d) at the strong temperature gradients (Fig. 2a) and resulting water
440 column stability maxima ($\sim 1 \times 10^{-3} \text{ s}^{-2}$).

441 Bin-averaged values of K_z varied by a factor of 5 , ranging from $6 \times 10^{-7} \text{ m}^2 \text{ s}^{-1}$
442 in the central interior to $3 \times 10^{-6} \text{ m}^2 \text{ s}^{-1}$ in the lower region of the transition layer (Fig.
443 4b). In the upper interface (thermocline – transition layer), where ϵ was elevated with
444 respect to the central interior but reduced compared to the lower interfacial layer,
445 stronger stratification (i.e., larger N^2 values up to 10^{-3} s^{-2}) reduced the eddy
446 diffusivities. At the interior-BBL, higher K_z values ($\sim 2 \times 10^{-5} \text{ m}^2 \text{ s}^{-1}$) resulted from
447 increased turbulence and weaker stratification. This enhanced turbulent transport was
448 located where the vertical O_2 gradient was the strongest (Fig. 2d).

449

450 3.3 Oxygen fluxes and budget

451 With the fast responding AMT galvanic O_2 sensor and rapid sampling rate, we
452 were able to resolve the O_2 gradient with high precision. Figure 4c shows the 2 m bin
453 average O_2 fluxes for the interior together with the averages from each ensemble.

Lorenzo Rovelli 23/12/2015 18:50

Deleted: as well as

Lorenzo Rovelli 23/12/2015 18:50

Deleted: in the center of the stratified interior.

Lorenzo Rovelli 23/12/2015 18:50

Deleted: TKE

Lorenzo Rovelli 23/12/2015 18:50

Deleted: a very

458 Small O₂ fluxes (~1 mmol m⁻² d⁻¹) were estimated for the center and upper region of
459 the interior; suggesting that relatively little O₂ is transported upward from the O₂
460 maximum to the upper interior. In contrast, a substantial O₂ flux ranging from 9 – 134
461 mmol m⁻² d⁻¹ (average of 54 mmol m⁻² d⁻¹) was identified from the lower thermocline
462 towards the BBL. The confidence interval associated with the uncertainties of the O₂
463 flux estimates was 18 – 74 mmol m⁻² d⁻¹. Although the O₂ fluxes to the BBL water
464 from the thermocline were variable in magnitude (Fig. 4c) and the measurements
465 limited to the observational period (Fig. 3), their magnitude nevertheless suggests an
466 important, yet overlooked, O₂ pathway.

467 We performed a simple 1-D BBL mass balance to investigate the relevance to
468 the local O₂ balance during our observational period. Here, we defined the apparent
469 (measured) O₂ loss rate in the BBL $\partial[O_2]/\partial t$ as the consequence of O₂ replenishment
470 from F_θ and the O₂ utilization via sediment O₂ uptake rate (SUR) and water column
471 organic matter respiration (R) expressed as

$$\frac{\partial[O_2]V}{\partial t A} = |F_\theta| - |SUR| - |R| \quad \{mmol m^{-2} d^{-1}\} \quad (6)$$

472 The mass balance was constrained to the (assumed) well-mixed 35 m deep BBL
473 section of area, $A = 1 m^2$ with a volume, $V = 35 m^3$. We further assumed negligible
474 horizontal O₂ gradients (as observed from the CTD casts), and thus a net zero
475 horizontal O₂ advective transport.

476 The average SUR for the same time period and location, obtained from parallel
477 eddy correlation measurements, was ~-10 mmol m⁻² d⁻¹ (McGinnis et al., 2014). The
478 SUR was consistent with the average SUR at Oyster Grounds reported by Neubacher
479 et al. (2011), -9.8 mmol m⁻² d⁻¹, and with modeled SUR s at the same site (average -8.6
480 mmol m⁻² d⁻¹; Meire et al., 2013). The apparent BBL O₂ loss of -0.42 $\mu mol kg^{-1} d^{-1}$
481 was determined from the POZ lander O₂ optode time series (Fig. 5a) over 52 hours,
482 ($R^2=0.60$). Though limited to our short observational period, the vertically integrated
483 apparent BBL O₂ loss was about -15 mmol m⁻² d⁻¹ and thus within 2% of the nearby
484 North Dogger average presented by Greenwood et al. (2010). Based on Eq. (6) and
485 using the observed BBL O₂ loss rate, F_θ and SUR , the water column respiration, R
486 was calculated to be ~-60 mmol m⁻² d⁻¹. This implies that without the O₂
487 replenishment, the apparent BBL O₂ loss would be ~-2 $\mu mol kg^{-1} d^{-1}$ and thus four
488 times higher than observed. Our results indicated that the total respiration in the

Lorenzo Rovelli 23/12/2015 18:50

Deleted: this suggested

Lorenzo Rovelli 23/12/2015 18:50

Deleted: rest of the

Lorenzo Rovelli 23/12/2015 18:50

Deleted:),

Lorenzo Rovelli 23/12/2015 18:50

Deleted: ,

Lorenzo Rovelli 23/12/2015 18:50

Deleted: as well as

494 bottom water was therefore $\sim 70 \text{ mmol m}^{-2} \text{ d}^{-1}$ ($SUR + R$), with about 14% of the
495 organic carbon mineralization occurring in the sediment and 86% in the BBL.

496

497 4 Discussion

498 During our three-day observational period, we found that the baroclinic near-
499 inertial wave in the interior was the main contributor to the detected enhanced shear
500 (Fig. 3d) and the observed elevated vertical O_2 flux to the BBL (Fig. 6). As near-
501 inertial waves decay after a few weeks, it should be noted that we observed a rather
502 special situation, and that vertical O_2 fluxes will not likely be as highly elevated
503 during periods when near-inertial waves are not present.

504 Within this context, we: 1) discuss the turbulent mechanisms leading to these
505 thermocline O_2 fluxes and mechanisms promoting the formation of the O_2 maximum
506 zone in terms of primary productivity; 2) discuss the implication for the local O_2 BBL
507 dynamics and carbon budget; 3) elaborate on factors that can ultimately influence O_2
508 depletion in the North Sea and other seasonally stratified shelf seas.

509

510 4.1 Thermocline mixing

511 The expansive North Sea thermocline ($1 - 5 \times 10^5 \text{ km}^2$; Meyer et al., 2011)
512 has been regarded as being in a state of marginal stability, where additional sources of
513 shear could lead to increased thermocline mixing (e.g., van Haren et al., 1999).
514 Itswire et al. (1989) showed that layers of strong shear are likely to be found where
515 strong stratification occurs. Generally, in the absence of varying topography and
516 sloping boundaries, the major sources of shear in the thermocline are considered to be
517 internal tides and near-inertial oscillations (see Rippeth, 2005). Sharples et al. (2007)
518 demonstrated that internal tidally-driven thermocline mixing enhanced diapycnal
519 nutrient fluxes, the overall productivity in the thermocline, and the associated carbon
520 export to the BBL.

521 The occurrence of near-inertial oscillations in shelf seas during the stratified
522 season has been reported in several studies from the North Sea (van Haren et al.,
523 1999; Knight et al., 2002) and in other shelf seas (e.g., Rippeth et al., 2002;
524 McKinnon and Gregg, 2005). During the presence of baroclinic inertial waves in the
525 water column, periods of enhanced shear have been observed in the western Irish Sea

Lorenzo Rovelli 23/12/2015 18:50

Deleted: at

Lorenzo Rovelli 23/12/2015 18:50

Deleted: will

Lorenzo Rovelli 23/12/2015 18:50

Deleted: those

Lorenzo Rovelli 23/12/2015 18:50

Deleted: speculate

Lorenzo Rovelli 23/12/2015 18:50

Deleted: In general, away from

Lorenzo Rovelli 23/12/2015 18:50

Deleted: also

Lorenzo Rovelli 23/12/2015 18:50

Deleted: as well as

Lorenzo Rovelli 23/12/2015 18:50

Deleted: as well as

Lorenzo Rovelli 23/12/2015 18:50

Deleted: taking the form of shear spikes occur approximately every inertial period and in bursts lasting several days

537 (Rippeth et al., 2009), the Celtic Sea (Palmer et al., 2008) and the northern North Sea
538 (Burchard and Rippeth, 2009). These take the form of shear spikes, which occur
539 approximately every inertial period and in bursts lasting several days.

540 While we mainly attributed the observed enhanced turbulent mixing to the
541 occurrence of a near-inertial wave, the site's physical setting has further implications
542 for mixing processes in the thermocline. In the northern hemisphere, sites with anti-
543 cyclonic tides, such as Tommeliten, are often characterized by an increased vertical
544 extension of the BBL, and higher BBL dissipation rates than comparable cyclonic
545 sites (see Simpson and Tinker, 2009). As a result of this enhanced BBL thickness, we
546 observed sporadically elevated thermocline turbulence resulting from tidal-driven
547 bottom turbulence propagating vertically towards the thermocline (Fig. 5b). A study
548 by Burchard and Rippeth (2009) also reported that short lived thermocline shear
549 spikes can arise due to the alignment of the surface wind stress, bulk shear, and bed
550 stress vectors in the presence of baroclinic near-inertial motions and barotropic tidal
551 currents. These mechanisms are stronger with anti-cyclonic tides. Although all the
552 features required for shear spike generation were present during the observational
553 period, the two-layer mechanism described by these authors would require a more
554 complex water column structure to be applicable to the Tommeliten site.

555 The site's water column structure clearly showed the occurrence of a 10 m
556 thick transition layer (Fig. 2a). This layer represents the region of the water column
557 where mixing turns from elevated in the SBL to strongly reduced in the interior
558 (Ferrari and Boccaletti, 2004). The transition layer is therefore an obligate pathway
559 for solute and heat exchange between SBL and the interior (Ferrari and Boccaletti,
560 2004; Rhein et al., 2010) and has been reported to be a region of enhanced shear and
561 near-inertial wave activity (Dohan and Davis, 2011). Although the presented data did
562 not allow quantification of the O₂ exchange across the transition layer, such
563 contribution might be considerable and thus highly relevant for the cycling of O₂ and
564 CO₂ in the upper water column, which in turn could have direct biological
565 implications.

566

567 4.2 BBL O₂ dynamics

568 Ultimately, observed O₂ depletion in the BBL of the central North Sea
569 depends on the supply of organic matter, the rate of carbon mineralization, and the

Lorenzo Rovelli 23/12/2015 18:50

Deleted: to

Lorenzo Rovelli 23/12/2015 18:50

Deleted: reduce

Lorenzo Rovelli 23/12/2015 18:50

Deleted: represents

Lorenzo Rovelli 23/12/2015 18:50

Deleted: also

Lorenzo Rovelli 23/12/2015 18:50

Deleted: a

575 flux of O₂ to the bottom water either from horizontal advection or turbulent vertical
576 transport. Our study investigated the significance of turbulent vertical O₂ fluxes to the
577 BBL, which has been previously overlooked in shelf sea carbon balances. Studies
578 focusing on O₂ replenishment in the BBL through the thermocline are limited to
579 freshwater systems (e.g. Bouffard et al., 2013; Kreling et al., 2014). In a large
580 stratified water body such as Lake Erie, O₂ transport from the thermocline to the
581 hypolimnion was found to be substantial, with a magnitude comparable to ~18% of
582 the hypolimnetic O₂ utilization rate over the whole stratification period (Bouffard et
583 al., 2013).

584 Horizontal O₂ gradients and associated horizontal advective O₂ fluxes were
585 not quantified in this study. Our data suggest, however, that such fluxes would not
586 significantly contribute to the O₂ balance at the Tommeliten site. BBL O₂
587 concentration time series (Fig. 5a) did not show any variability at the tidal and or
588 inertial frequencies, implying that horizontal O₂ gradients were small. Additionally,
589 mean currents in the BBL were small (~2 cm s⁻¹) compared to the tidal amplitudes.
590 This, in conjunction with weak horizontal O₂ gradients, suggests that horizontal
591 advective O₂ fluxes during our observational period are negligible compared to the
592 turbulent O₂ flux from the thermocline.

593 Based on the above, we can argue that the O₂ dynamics during the stratified
594 period are more complicated than previously regarded. To maintain an excess of O₂ in
595 the thermocline, primary producers require adequate nutrient entrainment from the
596 bottom water to fuel potential new production. The resulting increase in (new)
597 productivity and subsequent export to the bottom water could boost the carbon
598 turnover estimates substantially. Using a 1:1 O₂ utilization – carbon re-mineralization
599 (see Canfield, 1993), Greenwood et al. (2010) inferred the average BBL carbon re-
600 mineralization rate at the nearby North Dogger to be 15 mmol m⁻² d⁻¹, or 180 mg C m⁻²
601 d⁻¹. Similar results for a typical NW European shelf sea were obtained via modeling
602 by Sharples (2008), who reported rates ranging from ~35 to ~200 mg m⁻² d⁻¹ for neap
603 and spring tide, respectively. Their study, however, did not include the daily tidal
604 variation, and thus rates could be much higher on shorter timescales.

605 With the absence of targeted long-term studies focusing on O₂ and carbon
606 dynamics in the thermocline and BBL, we can only speculate on the long-term fate of
607 the BBL O₂ and its replenishment from the thermocline by vertical O₂ fluxes (F_{θ}). It

Lorenzo Rovelli 23/12/2015 18:50

Deleted: does

Lorenzo Rovelli 23/12/2015 18:50

Deleted: suggest

Lorenzo Rovelli 23/12/2015 18:50

Deleted: also

Lorenzo Rovelli 23/12/2015 18:50

Deleted: therefore

Lorenzo Rovelli 23/12/2015 18:50

Deleted: However, it

613 | seems possible, that the overall net BBL water column O₂ respiration, *R*, is higher than
614 | previously thought, suggesting a much higher carbon turnover than inferred from the
615 | apparent O₂ loss rate. Based on Eq. (6), the BBL carbon re-mineralization (and export
616 | to the BBL) would be on the order of nearly 850 mg C m⁻² d⁻¹, nearly a factor of 5
617 | higher than reported by Greenwood et al. (2010). However, the same turbulent
618 | transport that supports the O₂ export from the DCM to the BBL also supports BBL
619 | nutrient import to the DCM (Fig. 6). The higher import of nutrients to the DCM likely
620 | promotes additional primary production and a subsequent increase in organic matter
621 | (OM) export to the BBL. In such a scenario, the transient O₂ flux to the BBL
622 | presented in this study will be associated with additional OM to the BBL, and
623 | therefore lead to a temporary increased re-mineralization that offsets the increased *F_θ*.
624 | While the overall effect is an increase in carbon turnover, this process would not
625 | result in any observable change in the decreasing O₂ trend (apparent O₂ loss rate).

626

627 4.3 Causes and controls on BBL O₂ depletion

628 | According to Boers (2005), for BBL O₂ to decrease throughout the stratified
629 | season, there must be suitable physical conditions, biomass production, nutrient input
630 | and continued benthic O₂ uptake. *SUR*, and thus the sediment nutrient release and
631 | organic carbon mineralization have been shown to be strongly tidal-driven (McGinnis
632 | et al., 2014). Therefore, we briefly discuss the potential tidal impact driving the
633 | overall carbon cycling and suggest factors that may promote the development of
634 | lower BBL O₂ concentrations during the stratification period.

635 | Tidal forcing on diapycnal constituent fluxes and primary production have
636 | been explored by e.g., Sharples et al. (2007, 2008). The authors showed that spring-
637 | neap tide drives nutrient fluxes between the BBL and the DCM at the thermocline,
638 | and the carbon export. Based on our velocity measurements and estimated O₂ fluxes,
639 | we can expect similar patterns corresponding to semidiurnal tidal fluctuations. Blauw
640 | et al. (2012) investigated fluctuating phytoplankton concentrations in relation to tidal
641 | drivers and found that in the southern North Sea, chlorophyll fluctuations correlated
642 | with the typical tidal current speed periods, the semidiurnal tidal cycle, in addition to
643 | the day-night and spring-neap periods. During most of the year, chlorophyll and
644 | suspended particulate matter fluctuated in phase with tidal current speed, and indicated
645 | alternating periods of sinking and vertical mixing of algae and suspended matter with

Lorenzo Rovelli 23/12/2015 18:50

Deleted: over

Lorenzo Rovelli 23/12/2015 18:50

Deleted: almost

Lorenzo Rovelli 23/12/2015 18:50

Deleted: ephemeral

Lorenzo Rovelli 23/12/2015 18:50

Deleted: therefore does

Lorenzo Rovelli 23/12/2015 18:50

Deleted: as well as

Lorenzo Rovelli 23/12/2015 18:50

Deleted: also

Lorenzo Rovelli 23/12/2015 18:50

Deleted: that

Lorenzo Rovelli 23/12/2015 18:50

Deleted: ,

654 tidal cycles. Thus, these results suggest that in addition to the spring-neap tidal cycles,
655 we can expect a semidiurnal tidal-driven export of carbon and O₂ from the DCM to
656 the BBL, and entrainment of nutrients that strongly vary based on a timescale related
657 to the semi-diurnal tidal cycle.

658 The flux of O₂ from the DCM production zone downward to the BBL could
659 set the lower limit of the BBL O₂ concentration, and thus the O₂ depletion level,
660 during the stratification period. If there is little isolation between the zone of
661 production and the zone of mineralization, then the net O₂ production and O₂
662 utilization would nearly balance. In such case, the apparent O₂ loss in the BBL would
663 either be negligible or very small, depending whether the SUR, which is largely
664 particulate organic matter driven, will be balanced by the ventilation from the
665 thermocline. However, historically decreasing BBL O₂ concentrations within the
666 North Sea (Queste et al., 2013) point to an increasing disconnect between the primary
667 O₂ production zone and the mineralization zone. Greenwood et al. (2010) state that
668 stratification is an important factor which determines susceptibility to O₂ depletion,
669 especially in their nearby study site Oyster Grounds.

670 Surveys on the North Sea have shown that the regions with the lowest BBL O₂
671 concentrations are generally characterized by the strongest stratification (see Queste
672 et al., 2013), with the lowest values (~100 μmol kg⁻¹), reported to occur during
673 particularly calm and warm weather (see Boers, 2005; Weston et al., 2008). Strong
674 gradients in the thermocline associated with warmer temperature are suggested to
675 limit the O₂ flux to the BBL (Weston et al., 2008). This points to, potential future O₂
676 depletion resulting from increasing temperatures leading to both stronger stratification
677 and a longer stratification season (Lowe et al., 2009). However, it could be argued
678 that if O₂ fluxes between the DCM and BBL were suppressed, then the upward
679 nutrient fluxes would be similarly suppressed, thus inhibiting primary production and
680 reducing the potential for O₂ deficits.

682 4.4 Biological perspective

683 The occurrence of stronger stratification and subsequently reduced turbulent
684 mixing could alter algal populations (Hickman et al., 2009), potentially favoring
685 migrating/swimming phytoplankton. An example of these migrating phytoplankton
686 species, armored dinoflagellates, are extensively found in the DCM of the central and

Lorenzo Rovelli 23/12/2015 18:50

Deleted: the

Lorenzo Rovelli 23/12/2015 18:50

Deleted: as well as

Lorenzo Rovelli 23/12/2015 18:50

Deleted: , in addition to the spring-neap tidal cycles

Lorenzo Rovelli 23/12/2015 18:50

Deleted: particle

Lorenzo Rovelli 23/12/2015 18:50

Deleted: SUR

Lorenzo Rovelli 23/12/2015 18:50

Deleted: form

Lorenzo Rovelli 23/12/2015 18:50

Deleted: main

Lorenzo Rovelli 23/12/2015 18:50

Deleted: zones

Lorenzo Rovelli 23/12/2015 18:50

Deleted: and

Lorenzo Rovelli 23/12/2015 18:50

Deleted: reported

Lorenzo Rovelli 23/12/2015 18:50

Deleted: were also

Lorenzo Rovelli 23/12/2015 18:50

Deleted:), and point

Lorenzo Rovelli 23/12/2015 18:50

Deleted: the

Lorenzo Rovelli 23/12/2015 18:50

Formatted: Font color: Auto

Lorenzo Rovelli 23/12/2015 18:50

Deleted: expected

Lorenzo Rovelli 23/12/2015 18:50

Deleted: therefore not resulting in observed

Lorenzo Rovelli 23/12/2015 18:50

Deleted: might have much larger implications than presently thought, since

Lorenzo Rovelli 23/12/2015 18:50

Deleted: will

706 northern North Sea during the summer months; their abundance was found to be
707 largely determined by the local hydrodynamic conditions (Reid et al., 1990). In calm
708 conditions, which are typically associated with stronger stratification, there are often
709 blooms of migrating dinoflagellates which have access to the large nutrient pool in the
710 deeper water and can out-compete non-migrating species for both light and nutrients.
711 Stronger turbulent mixing, in contrast, has been suggested to interfere with their
712 swimming abilities (see Jephson et al., 2012 and references therein).

713 Algal migration could promote an upward shift of the DCM and move the
714 associated O₂ production higher in the thermocline, where turbulence levels are
715 reduced, while still maintaining comparable production rates. Even by a few meters,
716 such an upward shift would substantially reduce turbulent O₂ fluxes to the BBL and
717 likely further isolate the BBL from the potential O₂ supply in the thermocline,
718 although maintaining similar rates of carbon export (settling armored dinoflagellates).

719 Studies on climate change impacts on the North Sea have suggested that O₂
720 loss in the bottom waters would mainly result from a strengthening of the
721 stratification and O₂ solubility reduction with increasingly warmer waters (e.g., Meire
722 et al., 2013). In those scenarios, the intricate interplay between local tidally-driven
723 processes, water column structure, biogeochemical cycling and active phytoplankton
724 migration have not been considered nor quantified. The proposed mechanism could
725 contribute to the observed decreasing O₂ levels in the North Sea water column,
726 however, further detailed studies are obviously necessary to validate and fully
727 quantify this effect and the results described in this study, at the seasonal level.

729 Acknowledgements

730 We are thankful to the captain and crewmembers of the R/V *Celtic Explorer*
731 for their outstanding collaboration and support during the survey, Uwe Koy and
732 Rudolf Link for their logistic support, and Jens Schafstall, Tim Fischer and Markus
733 Faulhaber for their help in data collection and processing. We are grateful for the
734 technical development and support in deployment of the benthic chamber by Ralf
735 Schwarz, Sergiy Cherednichenko and the ROV Kiel 6000 team. Financial support was
736 provided by the Sonderforschungsbereich (SFB) 754 “Climate – Biogeochemistry in
737 the tropical Ocean”, SFB 574 “Volatiles and Fluids in Subduction Zones”, and by the
738 Excellence Cluster “Future Ocean” (project 2009/1 CP 0915, LR), supported by the

Lorenzo Rovelli 23/12/2015 18:50

Deleted: therefore

Lorenzo Rovelli 23/12/2015 18:50

Deleted: and thus favoring other algal species

Lorenzo Rovelli 23/12/2015 18:50

Deleted: Migration-driven movement

Lorenzo Rovelli 23/12/2015 18:50

Deleted: , even

Lorenzo Rovelli 23/12/2015 18:50

Deleted: means that the O₂ production will be shifted higher in the thermocline. Migrating phytoplankton could therefore access BBL nutrients in this scenario, i.e., primary production rates

Lorenzo Rovelli 23/12/2015 18:50

Deleted: be comparable, but the result would be an evident further decrease in the BBL O₂. For example, assuming our previous values of *SUR* and *R* in Eq. (6), but reducing *F_o* by half results in a nearly 3x increase in the apparent O₂ loss rate. Therefore, the combined effects of reduced

Lorenzo Rovelli 23/12/2015 18:50

Deleted: flux

Lorenzo Rovelli 23/12/2015 18:50

Deleted: a reduced O₂ gradient at the base of the thermocline, will both

Lorenzo Rovelli 23/12/2015 18:50

Deleted: this

Lorenzo Rovelli 23/12/2015 18:50

Deleted: while

Lorenzo Rovelli 23/12/2015 18:50

Deleted: We speculate that this mechanism could therefore provide a further loss of O₂ connectivity as the amount of production would remain approximately the same, but the supply of O₂ to the BBL would be substantially reduced. Of course, whether such scenario could be sustained over the whole stratification period is not known and requires further assessment. ... [3]

Lorenzo Rovelli 23/12/2015 18:50

Deleted: North Sea

Lorenzo Rovelli 23/12/2015 18:50

Deleted: The findings of this study suggest there might be an additional level of complexity based on

Lorenzo Rovelli 23/12/2015 18:50

Deleted: the

Lorenzo Rovelli 23/12/2015 18:50

Deleted: physics

Lorenzo Rovelli 23/12/2015 18:50

Deleted: in the central North Sea

773 Deutsche Forschungsgemeinschaft (DFG). Additional founding was provided by the
774 National Environmental Research Council (NERC, project NE/J011681/1). The cruise
775 was financed by Wintershall within the Fluid and Gas Seepage in the Southern
776 German North Sea (SDNS) project.
777

778 **References**

- 779 Batchelor, G. K.: The theory of homogeneous turbulence, Cambridge University
780 Press, Cambridge, 1953.
- 781 Best, M. A., Wither, A. W., and Coates, S.: Dissolved oxygen as a physico-chemical
782 supporting element in the Water Framework Directive, *Mar. Pollut. Bull.*, 55, 53–64,
783 doi:10.1016/j.marpolbul.2006.08.037, 2005.
- 784 Blauw, A. N., Beninca, E., Laane, R. W. P. M., Greenwood, N., and Huisman, J.:
785 Dancing with the tides: fluctuations of coastal phytoplankton orchestrated by different
786 oscillatory modes of the tidal cycle, *Plos One*, 7, e49319,
787 doi:10.1371/journal.pone.0049319, 2012.
- 788 Boers, M.: Effects of a deep sand extraction pit. Final report of the PUTMOR
789 measurements at the Lowered Dump Site, Rijkswa- terstaat, The Netherlands,
790 RIKZ/2005.001, 87, 2005.
- 791 Bouffard, D., Ackerman, J. D., and Boegman, L.: Factors affecting the development
792 and dynamics of hypoxia in a large shallow stratified lake: hourly to seasonal
793 patterns, *Water Resour. Res.*, 49, 2380–2394, doi:10.1002/wrcr.20241, 2013.
- 794 Brandt, P., Bange, H., Banyte, D., Dengler, M., Didwischus, S-H., Fischer, T.,
795 Greatbatch, R., Hahn, J., Kanzow, T., Karstensen, J., Körtzinger, A., Krahnmann, G.,
796 Schmidtko, S., Stramma, L., Tanhua T., and Visbeck, M.: On the role of circulation
797 and mixing in the ventilation of oxygen minimum zones with a focus on the eastern
798 tropical North Atlantic, *Biogeosciences*, 12, 489–512, doi:10.5194/bg-12-489-2015,
799 2015.
- 800 Burchard, H., and Rippeth, T. P.: Generation of bulk shear spikes in shallow stratified
801 tidal seas, *J. Phys. Oceanogr.*, 39, 969–985, doi:10.1175/2008JPO4074.1, 2009.
- 802 Canfield, D. E.: Organic matter oxidation in marine sediments, in: *Interactions of C,*
803 *N, P and S biogeochemical cycles and global change*, edited by: Wollast, R.,
804 Mackenzie, F. T., and Chou, L., Springer, Berlin, 333–363, 1993.
- 805 Chan, F., Barth, J. A., Lubchenco, J., Kirincich, A., Weeks, H., Peterson, W. T., and
806 Menge, B. A.: Emergence of anoxia in the California current large marine ecosystem,
807 *Science*, 319, 920–920, doi:10.1126/Science.1149016, 2008.

808 Crawford, W. R., and Pena, M. A.: Declining oxygen on the British Columbia
809 continental shelf, *Atmos. Ocean.*, 51, 88–103, doi:10.1080/07055900.2012.753028,
810 2013.

811 Diaz, R. J.: Overview of hypoxia around the world, *J. Environ. Qual.*, 30, 275–281,
812 doi:10.2134/jeq2001.302275x, 2001.

813 Diaz, R. J., and Rosenberg, R. : Spreading dead zones and consequences for marine
814 ecosystems, *Science*, 321, 926–929, doi:10.1126/Science.1156401, 2008.

815 Dohan, K, and Davis, R. E.: Mixing in the transition layer during two storm events, *J.*
816 *Phys. Oceanogr.*, 41, 42–66, doi:10.1175/2010jpo4253.1, 2011.

817 Efron, B.: 1977 Rietz lecture - bootstrap methods - another look at the jackknife, *Ann.*
818 *Stat.*, 7, 1–26, 1979.

819 Ferrari, R., and Boccaletti, G.: Eddy-mixed layer interactions in the ocean,
820 *Oceanography*, 17, 12–21, doi:10.5670/oceanog.2004.26. 2004.

821 Ferrari, R., and Polzin, K. L.: Finescale structure of the T-S relation in the eastern
822 North Atlantic, *J. Phys. Oceanogr.*, 35, 1437–1454, doi:10.1175/JPO2763.1, 2005.

823 Fischer, T., Banyte, D., Brandt, P., Dengler, M., Krahnemann, G., Tanhua, T., and
824 Visbeck, M.: Diapycnal oxygen supply to the tropical North Atlantic oxygen
825 minimum zone, *Biogeosciences*, 10, 5079–5093, doi:10.5194/bg-10-5079-2013, 2013.

826 Fofonoff, N. P.: Physical properties of seawater: A new salinity scale and equation of
827 state for seawater, *J. Geophys. Res.*, 90, 3332–3342, doi:10.1029/Jc090ic02p03332,
828 1985.

829 Glud, R. N.: Oxygen dynamics of marine sediments, *Mar. Biol. Res.*, 4, 243–289,
830 doi:10.1080/17451000801888726, 2008.

831 Grantham, B. A., Chan, F., Nielsen, K. J., Fox, D. S., Barth, J. A., Huyer, A.,
832 Lubchenco, J., and Menge, B. A.: Upwelling-driven nearshore hypoxia signals
833 ecosystem and oceanographic changes in the northeast Pacific, *Nature*, 429, 749–754,
834 doi:10.1038/Nature02605, 2004.

835 Greenwood, N., Parker, E. R., Fernand, L., Sivyer, D. B., Weston, K., Painting, S. J.,
836 Kroger, S., Forster, R. M., Lees, H. E., Mills, D. K., and Laane, R. W. P. M.:
837 Detection of low bottom water oxygen concentrations in the North Sea; implications

838 for monitoring and assessment of ecosystem health, *Biogeosciences*, 7, 1357–1373,
839 doi:10.5194/bg-7-1357-2010, 2010.

840 Hickman, A. E., Holligan, P. M., Moore, C. M., Sharples, J., Krivtsov, V., and
841 Palmer, M. R.: Distribution and chromatic adaptation of phytoplankton within a shelf
842 sea thermocline, *Limnol. Oceanogr.*, 54, 525–536, doi:10.4319/lo.2009.54.2.0525,
843 2009.

844 Hovland, M., and Judd, A.: *Seabed pockmarks and seepage: Impact on geology,
845 biology and the marine environment*, Graham and Trotman, London, 1988.

846 Itsweire, E. C., Osborn, T. R., and Stanton, T. P.: Horizontal distribution and
847 characteristics of shear layers in the seasonal thermocline, *J. Phys. Oceanogr.*, 19,
848 302–320, doi:10.1175/1520-0485(1989)019<0301:HDACOS>2.0.CO;2, 1989.

849 Ivey, G. N., and Imberger, J.: On the nature of turbulence in a stratified fluid, Part I:
850 The energetics of mixing, *J. Phys. Oceanogr.*, 21, 650–658, doi:10.1175/1520-
851 0485(1991) 021<0650:OTNOTI>2.0.CO;2, 1991.

852 Jephson, T., Carlsson, P., and Fagerberg, T.: Dominant impact of water exchange and
853 disruption of stratification on dinoflagellate vertical distribution, *Estuarine, Coastal
854 Shelf Sci.*, 112, 198–206, doi:10.1016/j.ecss.2012.07.020, 2012.

855 Jørgensen, B. B., and Revsbech, N. P.: Diffusive boundary layers and the oxygen
856 uptake of sediments and detritus, *Limnol. Oceanogr.*, 30, 111–122,
857 doi:10.4319/lo.1985.30.1.0111, 1985.

858 Kemp, W. M., Testa, J. M., Conley, D. J., Gilbert, D., and Hagy, J. D.: Temporal
859 responses of coastal hypoxia to nutrient loading and physical controls,
860 *Biogeosciences*, 6, 2985–3008, doi:10.5194/bg-6-2985-2009, 2009.

861 Knight, P. J., Howarth, M. J., and Rippeth, T. P.: Inertial currents in the northern
862 North Sea, *J. Sea Research*, 47, 269–284, doi:10.1016/S1385-1101(02)00122-3, 2002.

863 Kreling, J., Bravidor, J., McGinnis, D. F., Koschorreck, M., and Lorke, A.: Physical
864 controls of oxygen fluxes at pelagic and benthic oxyclines in a lake, *Limnol.
865 Oceanogr.*, 59, 1637–1650, doi:10.4319/lo.2014.59.5.1637, 2014.

866 Lorke, A., Umlauf, L., and Mohrholz, V.: Stratification and mixing on sloping
867 boundaries, *Geophys. Res. Lett.*, 35, L14610, doi:10.1029/2008GL034607, 2008.

868 Lowe, J. A., Howard, T. P., Pardaens, A., Tinker, J., Holt, J., Wakelin, S., Milne, G.,
869 Leake, J., Wolf, J., Horsburgh, K., Reeder, T., Jenkins, G., Ridley, J., Dye, S., and
870 Bradley, S.: UK Climate Projections science report: Marine and coastal projections.
871 Met Office Hadley Centre, available at:
872 <http://ukclimateprojections.metoffice.gov.uk/22530>, 2009.

873 MacKinnon, J. A., and Gregg, M. C.: Near-inertial waves on the New England shelf:
874 The role of evolving stratification, turbulent dissipation, and bottom drag, *J. Phys.*
875 *Oceanogr.*, 35, 2408–2424, doi:10.1175/JPO2822.1, 2005.

876 McGinnis, D. F., Sommer, S., Lorke, A., Glud, R. N., and Linke, P.: Quantifying
877 tidally driven benthic oxygen exchange across permeable sediments: An aquatic eddy
878 correlation study, *J. Geophys. Res.: Oceans*, 119, 6918–6932,
879 doi:10.1002/2014JC010303, 2014.

880 Meire, L., Soetaert, K. E. R., and Meysman, F. J. R.: Impact of global change on
881 coastal oxygen dynamics and risk of hypoxia, *Biogeosciences*, 10, 2633–2653,
882 doi:10.5194/bg-10-2633-2013, 2013.

883 Meyer, E. M. I., Pohlmann, T., and Wiese, R.: Thermodynamic variability and
884 change in the North Sea (1948-2007) derived from a multidecadal hindcast, *J. Mar.*
885 *Syst.*, 86, 35–44, doi:10.1016/j.jmarsys.2011.02.001, 2011.

886 Neubacher, E. C., Parker, R. E., and Trimmer, M.: Short-term hypoxia alters the
887 balance of the nitrogen cycle in coastal sediments, *Limnol. Oceanogr.*, 56, 651–665,
888 doi:10.4319/lo.2011.56.2.0651, 2011.

889 North Sea Task Force: North Sea Quality Status Report, Report No.: 1 872349 05 6,
890 London: Oslo and Paris Commissions, 1993.

891 Osborn, T. R.: Estimates of the local rate of vertical diffusion from dissipation
892 measurements, *J. Phys. Oceanogr.*, 10, 83–89, doi:10.1175/1520-
893 0485(1980)010<0083: EOTLRO>2.0.CO;2, 1980.

894 OSPAR (Oslo-Paris convention for the protection of the marine environment of the
895 North-East Atlantic): EcoQO Handbook—Handbook for the application of ecological
896 quality objectives in the North Sea, Report No.: 978-1-905859-46-7, 2nd edn.,
897 OSPAR Biodiversity Series 2009/307, available at
898 http://www.ospar.org/v_publications/browse.asp, 2009.

899 OSPAR: Quality Status Report 2010, Report No: 978-1-906840-44-0, OSPAR
900 Commission, London, available at <http://qsr2010.ospar.org/en/index.html>, 2010.

901 Otto, L., Zimmerman, J. T. F., Furnes, G. K., Mork, M., Saetre, R., and Becker, G.:
902 Review of the physical oceanography of the North Sea, *Ned. J. Sea Res.*, 26, 161–
903 238, doi:10.1016/0077-7579(90)90090-4, 1990.

904 Palmer, M. R., Rippeth, T. P., and Simpson, J. H.: An investigation of internal mixing
905 in a seasonally stratified shelf sea, *J. Geophys. Res.*, 113, C12005,
906 doi:10.1029/2007JC004531, 2008.

907 Pfannkuche, O., Linke, P.: GEOMAR landers as long-term deep-sea observatories,
908 *Sea Technol.* 44, 50–55, 2003.

909 Pingree, R. D., Holligan, P. M., and Mardell, G. T.: The effect of vertical stability on
910 phytoplankton distributions in the summer on the Northwest European Shelf, *Deep*
911 *Sea Res.*, 25, 1011–1028, doi:10.1016/0146-6291(78)90584-2, 1978.

912 Prandke, H., and Stips, A.: Test measurements with an operational microstructure-
913 turbulence profiler: Detection limit of dissipation rates, *Aquat. Sci.*, 60, 191–209,
914 doi:10.1007/s000270050036, 1998.

915 Queste, B.Y., Fernand, L., Jickells, T. D., and Heywood, K. J.: Spatial extent and
916 historical context of North Sea oxygen depletion in August 2010, *Biogeochemistry*,
917 113, 53–68, doi:10.1007/s10533-012-9729-9, 2013.

918 Radach, G. and Lenhart, H. J.: Nutrient dynamics in the North Sea: Fluxes and
919 budgets in the water column derived from ERSEM, *Neth. J. Sea Res.*, 33, 301–335,
920 doi:10.1016/0077-7579(95)90051-9, 1995

921 Reid, P. C., Lancelot, C., Gieskes, W. W. C., Hagmeier, E., and Weichart, G.:
922 Phytoplankton of the North Sea and its dynamics - a review, *Neth. J. Sea Res.*, 26,
923 295–331, doi:10.1016/0077-7579(90)90094-W, 1990.

924 Rhein, M., Dengler, M., Sültenfuß, J., Hummels, R., Hüttl-Kabus, S., and Bourles, B.:
925 Upwelling and associated heat flux in the equatorial Atlantic inferred from helium
926 isotope disequilibrium, *J. Geophys. Res.*, 115, C08021, doi:10.1029/2009JC005772,
927 2010.

928 Rippeth, T. P.: Mixing in seasonally stratified shelf seas: A shifting paradigm, *Phil.*
929 *Trans. R. Soc. A*, 363, 2837–2854, doi:10.1098/rsta.2005.1662, 2005.

930 Rippeth, T. P., Simpson, J. H., Player, R., and Garcia, M. C.: Current oscillations in
931 the diurnal-inertial band on the Catalanian Shelf in spring, *Cont. Shelf Res.*, 22, 247–
932 265, doi:10.1016/S0278-4343(01)00056-5, 2002.

933 Rippeth, T. P., Wiles, P., Palmer, M. R., Sharples, J., and Tweddle, J.: The diapycnal
934 nutrient flux and shear-induced diapycnal mixing in the seasonally stratified western
935 Irish Sea, *Cont. Shelf Res.*, 29, 1580–1587, doi:10.1016/j.csr.2009.04.009, 2009.

936 Schafstall, J., Dengler, M., Brandt, P., and Bange, H.: Tidal-induced mixing and
937 diapycnal nutrient fluxes in the Mauritanian upwelling region, *J. Geophys. Res.:*
938 *Oceans*, 115, C10014, doi:10.1029/2009jc005940, 2010.

939 Sharples, J.: Potential impacts of the spring-neap tidal cycle on shelf sea primary
940 production, *J. Plankton Res.*, 30, 183–197, doi: 10.1093/plankt/fbm088, 2008.

941 Sharples, J., Moore, C. M., Rippeth, T. P., Holligan, P. M., Hydes, D. J., Fisher, N.
942 R., and Simpson, J. H.: Phytoplankton distribution and survival in the thermocline,
943 *Limnol. Oceanogr.*, 46, 486–496, doi:10.4319/lo.2001.46.3.0486, 2001.

944 Sharples, J., Tweddle, J. F., Green, J. A. M., Palmer, M. R., Kim, Y. N., Hickman, A.
945 E., Holligan, P. M., Moore, C. M., Rippeth, T. P., Simpson, J. H., and Krivtsov, V.:
946 Spring-neap modulation of internal tide mixing and vertical nitrate fluxes at a shelf
947 edge in summer, *Limnol. Oceanogr.*, 52, 1735–1747, doi: 10.4319/lo.2007.52.5.1735,
948 2007.

949 Schneider von Deimling, J., Greinert, J., Chapman, N. R., Rabbel, W., and Linke, P.:
950 Acoustic imaging of natural gas bubble ebullition in the North Sea: Sensing the
951 temporal, spatial and activity variability, *Limnol. Oceanogr.: Methods*, 8, 155–171,
952 doi:10.4319/ lom.2010.8.155, 2010.

953 Shih, L. H., Koseff, J. R., Ivey, G. N., and Ferziger, J. H.: Parameterization of
954 turbulent fluxes and scales using homogeneous sheared stably stratified turbulence
955 simulations, *J. Fluid Mech.*, 525, 193–214, doi:10.1017/S0022112004002587, 2005.

956 Simpson, J. H., and Tinker, J. P.: A test of the influence of tidal stream polarity on the
957 structure of turbulent dissipation, *Cont. Shelf Res.*, 29, 320–332, doi:10.1016/
958 j.csr.2007.05.013, 2009.

959 Smyth, W. D., Moum, J. N., and Caldwell, D. R.: The efficiency of mixing in
960 turbulent patches: inferences from direct simulations and microstructure observations,

961 J. Phys. Oceanogr., 31, 1969–1992, doi:10.1175/1520-
962 0485(2001)031<1969:TEOMIT>2.0.CO;2, 2001.

963 St. Laurent, L., and Schmitt, R. W.: The contribution of salt fingers to vertical mixing
964 in the North Atlantic Tracer Release Experiment, J. Phys. Oceanogr., 29, 1404–1424,
965 1999.

966 Thomas, H., Bozec, Y., de Baar, H. J. W., Elkalay, K., Frankignoulle, M.,
967 Schiettecatte, L.-S., Kattner, G., and Borges, A. V.: The carbon budget of the North
968 Sea, Biogeosciences, 2, 87–96, doi:10.5194/bg-2-87-2005, 2005.

969 van Haren, H., Mass, L., Zimmerman, J. T. R., Ridderinkhof, H., and Malschaert, H.:
970 Strong inertial currents and marginal internal wave stability in the central North Sea,
971 Geophys. Res. Lett., 26, 2993–2996, doi:10.1029/1999GL002352, 1999.

972 Vaquer-Sunyer, R., and Duarte, C. M.: Thresholds of hypoxia for marine biodiversity,
973 P. Natl. Acad. Sci. USA., 105, 15452–15457, doi:10.1073/pnas.0803833105, 2008.

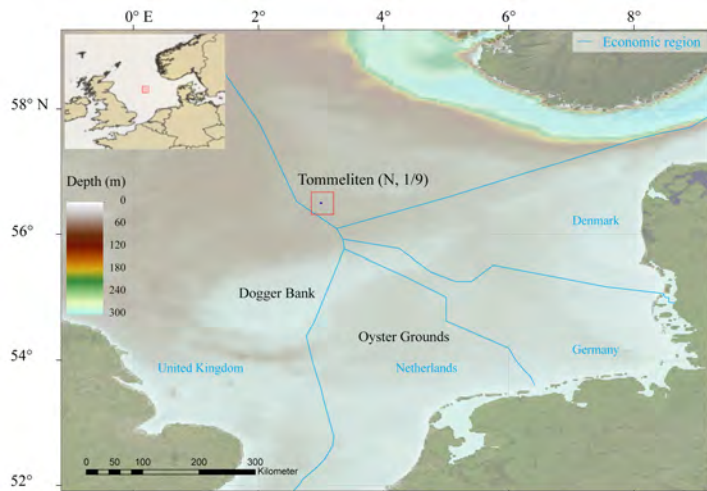
974 Wanninkhof, R.: Relationship between wind speed and gas exchange over the ocean,
975 J. Geophys. Res.: Oceans, 97, 7373–7382, doi:10.1029/92jc00188, 1992

976 Weston, K., Fernand, L., Mills, D. K., Delahunty, R., and Brown, J.: Primary
977 production in the deep chlorophyll maximum of the central North Sea, J. Plankton
978 Res., 27, 909–922, doi:10.1093/plankt/fbi064, 2005.

979 Weston, K., Greenwood, N., Fernand, L., Pearce, D. J., and Sivyer, D. B.:
980 Environmental controls on phytoplankton community composition in the Thames
981 plume, U.K. J. Sea Res., 60, 246–254, doi:10.1016/j.seares.2008.09.003, 2008.

982 [Winkler, L., Die Bestimmung des in Wasser Gelösten Sauerstoffes, Berichte der](#)
983 [Deutschen Chemischen Gesellschaft, 21, 2843–2855, 1888.](#)

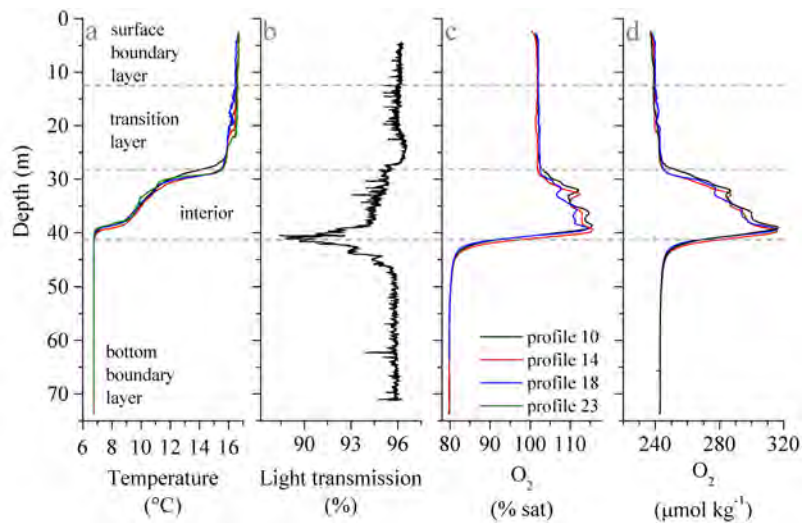
984



985
986

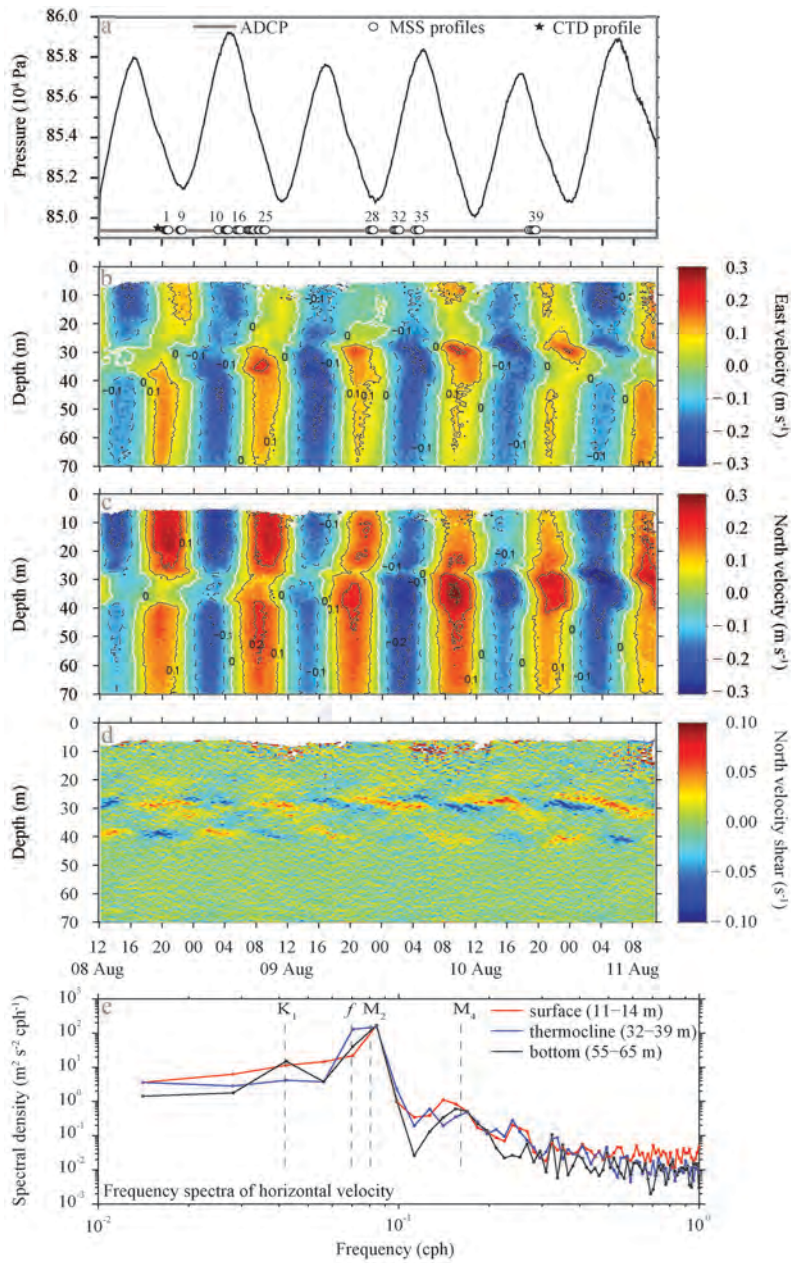
987 Figure 1. Map of the North Sea indicating the water depths and location of the
988 Tommeliten site and the borders of the economic regions of the surrounding European
989 countries.

Lorenzo Rovelli 23/12/2015 18:50
Deleted: as well as



991
992

993 Figure 2. Selected water column profiles based on based on high-resolution MSS
 994 profiles (a, c, d) and ship CTD profile (b). (a) Potential temperature profiles. Water
 995 column layers were identified based on the temperature profiles. A 0.2°C and 1.5°C
 996 decrease from the surface boundary layer average temperature (3–6 m depth) was
 997 used determine the depth of the surface boundary layer – transition layer interface and
 998 the transition layer – interior interface, respectively. Correspondingly, a 0.2°C from a
 999 50-60 m depth average temperature was used to locate the interior – bottom boundary
 1000 layer interface. (b) Light transmission profile. (c, d) O₂ saturation profiles and
 1001 associated absolute concentrations.



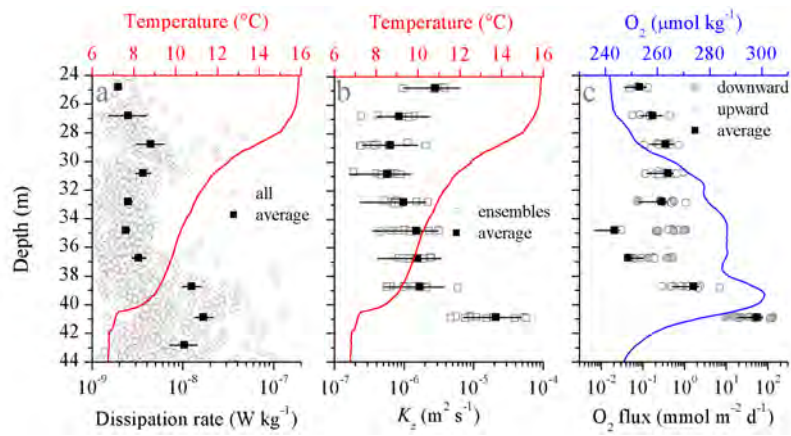
1002
1003

1004 Figure 3. Current regime at the Tommeliten site from ADCP measurements (a - d)
1005 and spectral analysis (e). (a) Sea surface elevation relative to average level during the
1006 observational period (elevation = 0 m) and schedule of different instrument

1007 deployments. Numbers on the MSS markers indicate the profile number. (b, c)
1008 Horizontal velocities, showing 20 min averaged east (b) and north (c) velocities. (d)
1009 Vertical shear of North velocity, dv/dz , calculated from the ADCP velocity data (see
1010 panels b, c). Note that panels a - d have the same time axis. (e) Frequency spectra of
1011 horizontal velocity calculated from the ADCP data for selected depth ranges for the
1012 SBL (surface; red line), thermocline (blue line), and BBL (bottom; black line). The
1013 inertial f_c , K_1 , M_2 and M_4 frequencies are marked.

Lorenzo Rovelli 23/12/2015 18:50

Deleted: as well as the



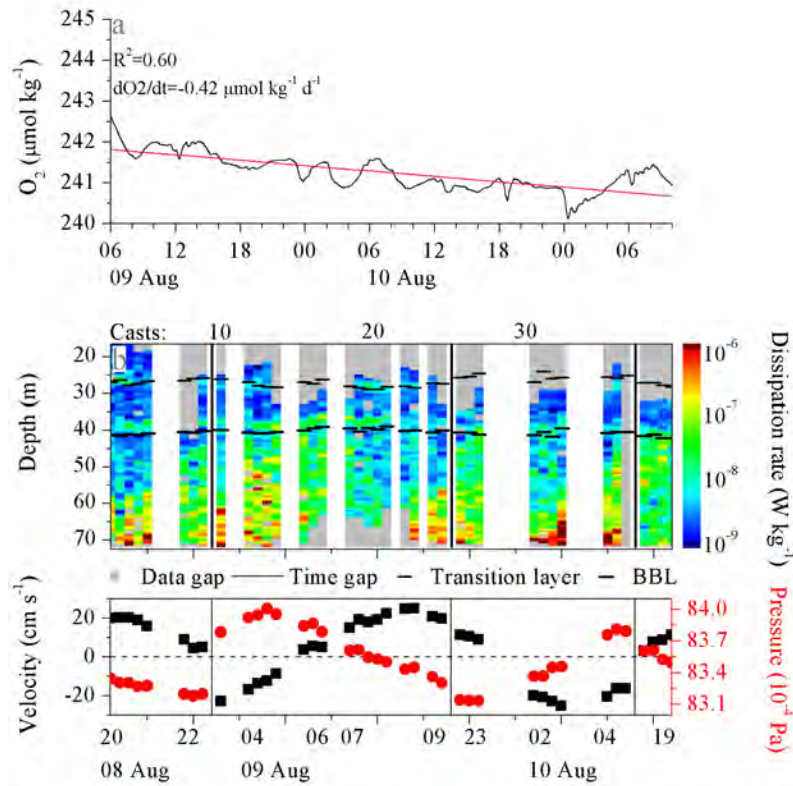
1015
1016

1017 Figure 4. Overview of turbulent transport and O₂ fluxes within the interior (defined in
1018 Fig. 2). Each panel is overlaid with temperature (a, b) and O₂ concentration (c)
1019 profiles. (a) Dissipation from all profiles (open dots) together with the arithmetic
1020 mean (solid squares). (b) Average vertical eddy diffusion coefficient K_z with
1021 uncertainties bars and the K_z values for every ensemble (open squares), which
1022 represent the average over 3 to 4 consecutive profiles. (c) Calculated average O₂ flux
1023 over 2 m bins with the respective uncertainties intervals (solid square and black line).
1024 The values for each profile cluster are shown both downward and upward fluxes (grey
1025 solid and open dots, respectively). Note that in the center interior (33 – 37 m) the
1026 average reflects the combination of the variability of the observed upward and
1027 downwards fluxes.

1028

Lorenzo Rovelli 23/12/2015 18:50

Deleted: as well as



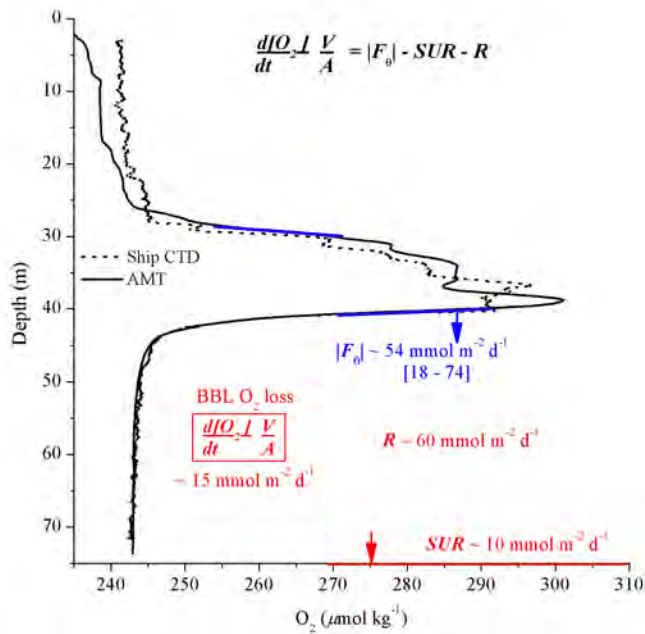
1030

1031

1032 Figure 5. BBL dissolved oxygen time series and turbulence contour. (a) Near-seafloor
 1033 BBL O_2 concentration changes over the observational period from the POZ-Lander.
 1034 Red line indicates the estimated apparent linear O_2 loss. (b, top) Turbulence contour
 1035 plot of all MSS90 casts together with the temperature layers. Thin and thick dashed
 1036 lines represent the transition layer – interior interface and the interior – BBL interface,
 1037 respectively. Gray spots indicate data missing due to uncompleted profiles (casts 16-
 1038 23), unsuccessful profiles (cast 36), or flagged as bad based on spikes, collisions and
 1039 suspected contamination due to ship activity. The vertical black lines indicate the
 1040 transition (time gaps) between consecutive profile ensembles. (b, bottom) Background
 1041 information on bottom current, and hydrostatic pressure during the casts. Both
 1042 velocity and pressure data were collected by the deployed POZ lander. Note that as a
 1043 result of the time gaps between the consecutive MSS90 casts (see Fig. 3a) the time
 1044 scale is not linear.

1045

1046



1047

1048

1049 Figure 6. Main O_2 fluxes in this study. The ranges shown for the interior O_2 fluxes
1050 refer to the associated uncertainty and intermittency levels. The sediment O_2 uptake
1051 rates (SUR)

1052 are based on eddy correlation (EC) measurements (McGinnis et al., 2014), while
1053 central North Sea apparent BBL O_2 loss is based on Greenwood et al. (2010) and this
1054 study. Representative O_2 profiles are based on the AMT sensor on the MSS profiler
1055 (solid line) and ship CTD (dotted line). Note that while the O_2 profiles showed
1056 differences in absolute concentration within the thermocline, the actual O_2 gradients
1057 within the thermocline-BBL oxycline are comparable.

Page 1: [1] Deleted **Lorenzo Rovelli** **23/12/2015 18:50**

the

Page 1: [1] Deleted **Lorenzo Rovelli** **23/12/2015 18:50**

the

Page 1: [1] Deleted **Lorenzo Rovelli** **23/12/2015 18:50**

the

Page 1: [1] Deleted **Lorenzo Rovelli** **23/12/2015 18:50**

the

Page 1: [1] Deleted **Lorenzo Rovelli** **23/12/2015 18:50**

the

Page 1: [1] Deleted **Lorenzo Rovelli** **23/12/2015 18:50**

the

Page 1: [1] Deleted **Lorenzo Rovelli** **23/12/2015 18:50**

the

Page 1: [1] Deleted **Lorenzo Rovelli** **23/12/2015 18:50**

the

Page 1: [1] Deleted **Lorenzo Rovelli** **23/12/2015 18:50**

the

Page 1: [1] Deleted **Lorenzo Rovelli** **23/12/2015 18:50**

the

Page 1: [1] Deleted **Lorenzo Rovelli** **23/12/2015 18:50**

the

Page 1: [1] Deleted **Lorenzo Rovelli** **23/12/2015 18:50**

the

Page 1: [1] Deleted **Lorenzo Rovelli** **23/12/2015 18:50**

the

Page 1: [2] Deleted **Lorenzo Rovelli** **23/12/2015 18:50**

the

Page 1: [2] Deleted **Lorenzo Rovelli** **23/12/2015 18:50**

the

Page 1: [2] Deleted **Lorenzo Rovelli** **23/12/2015 18:50**

the

Page 1: [2] Deleted **Lorenzo Rovelli** **23/12/2015 18:50**

the

Page 1: [2] Deleted **Lorenzo Rovelli** **23/12/2015 18:50**

the

Page 1: [2] Deleted **Lorenzo Rovelli** **23/12/2015 18:50**

the

Page 1: [2] Deleted **Lorenzo Rovelli** **23/12/2015 18:50**

the

Page 1: [2] Deleted **Lorenzo Rovelli** **23/12/2015 18:50**

the

Page 1: [2] Deleted **Lorenzo Rovelli** **23/12/2015 18:50**

the

Page 1: [2] Deleted **Lorenzo Rovelli** **23/12/2015 18:50**

the

Page 1: [2] Deleted **Lorenzo Rovelli** **23/12/2015 18:50**

the

Page 1: [2] Deleted **Lorenzo Rovelli** **23/12/2015 18:50**

the

Page 1: [2] Deleted **Lorenzo Rovelli** **23/12/2015 18:50**

the

the

the

the

We speculate that this mechanism could therefore provide a further loss of O₂ connectivity as the amount of production would remain approximately the same, but the supply of O₂ to the BBL would be substantially reduced. Of course, whether such scenario could be sustained over the whole stratification period is not known and requires further assessment.

In the light of climatic changes, studies